PNAS RESEARCH ARTICLE | CELL BIOLOGY

Ezh2 promotes mammary tumor initiation through epigenetic regulation of the Wnt and mTORC1 signaling pathways

Linshan Liu[a,b], Bin Xiao[a,b], Alison Hirukawa[a,b], Harvey W. Smith[a], Dongmei Zuo[a,b], Virginie Sanguin-Gendreau[a], Luke McCaffrey[b,c,d], Alice Jisoo Nam[a,b], and William J. Muller[a,b,c,1]

Edited by Kornelia Polyak, Dana-Farber Cancer Institute, Boston, MA; received February 28, 2023; accepted June 22, 2023

The regulation of gene expression through histone posttranslational modifications plays a crucial role in breast cancer progression. However, the molecular mechanisms underlying the contribution of histone modification to tumor initiation remain unclear. To gain a deeper understanding of the role of the histone modifier Enhancer of Zeste homology 2 (Ezh2) in the early stages of mammary tumor progression, we employed an inducible mammary organoid system bearing conditional *Ezh2* alleles that faithfully recapitulates key events of luminal B breast cancer initiation. We showed that the loss of Ezh2 severely impairs oncogene-induced organoid growth, with Ezh2-deficient organoids maintaining a polarized epithelial phenotype. Transcriptomic profiling showed that Ezh2-deficient mammary epithelial cells up-regulated the expression of negative regulators of Wnt signaling and down-regulated genes involved in mTORC1 (mechanistic target of rapamycin complex 1) signaling. We identified *Sfrp1*, a Wnt signaling suppressor, as an Ezh2 target gene that is derepressed and expressed in Ezh2-deficient epithelium. Furthermore, an analysis of breast cancer data revealed that *Sfrp1* expression was associated with favorable clinical outcomes in luminal B breast cancer patients. Finally, we confirmed that targeting Ezh2 impairs mTORC1 activity through an indirect mechanism that up-regulates the expression of the tumor suppressor Pten. These findings indicate that Ezh2 integrates the mTORC1 and Wnt signaling pathways during early mammary tumor progression, arguing that inhibiting Ezh2 or therapeutically targeting Ezh2-dependent programs could be beneficial for the treatment of early-stage luminal B breast cancer.

breast cancer | EZH2 | tumor initiation | Wnt signaling | mTOR signaling

Significance

Although breast cancer is a leading cause of death in women, the molecular mechanisms underlying its initiation remain unclear. This study provides insights into the role of the histone modifier Ezh2 in early mammary tumor progression. The findings suggest that Ezh2 plays a crucial role in integrating the mTORC1 and Wnt signaling pathways to initiate mammary tumor progression. Specifically, loss of Ezh2 up-regulated genes involved in suppressing these pathways. Notably, Sfrp1, a negative regulator of Wnt signaling, was up-regulated in Ezh2-deficient epithelium, and its expression was associated with favorable clinical outcomes in luminal B subtype patients. Overall, this study highlights the importance of epigenetics in breast cancer and identifies potential therapeutic targets.

Breast cancer is a heterogeneous disease that can be classified into at least six major molecular subtypes: luminal A, luminal B, HER2-positive, normal-like, claudin-low, and basal-like breast cancer (1–4). Although a large amount of work has explored the genetic alterations that drive tumor progression, emerging evidence has shown that the epigenetic regulation of oncogenic signaling pathways also plays a crucial role in this process (5, 6). Moreover, while correcting oncogenic mutations is challenging, the reversible nature of epigenetic regulation makes it a promising avenue for therapeutically targeting the cancer genome (7). DNA methylation and diverse posttranslational modifications of histones have been implicated as epigenetic mechanisms involved in cancer. The histone-modifying Polycomb repressive complex 2 (PRC2), composed of the four major subunits SUZ12, EED, RbAp46/48, and EZH2, controls the differentiation and proliferation of normal cells (8) and has been shown to play context-dependent oncogenic and tumor suppressive roles in cancer (9). As the core catalytic subunit of PRC2, EZH2 is a histone methyltransferase that facilitates the di- or trimethylation of histone H3 on lysine 27 (H3K27me2/3) (3, 4, 10). Interestingly, *EZH2* has been shown to act as an oncogene in various breast cancer subtypes (11–13), and elevated levels of EZH2 expression are associated with increased breast cancer aggressiveness (14). However, EZH2 can also exert tumor suppressive functions depending on estrogen receptor (ER) status (15). The distinct biological behavior of different breast cancer subtypes highlights the importance of investigating the role of Ezh2 in each molecular subtype of breast cancer.

To further dissect the molecular mechanisms underlying the role of EZH2 in breast cancer, genetically engineered mouse models (GEMMs) recapitulating mammary tumor progression are highly useful tools. Mammary epithelial-specific expression of the viral oncogene Polyomavirus middle T antigen (PyV mT) is sufficient to drive the formation of mammary tumors that transcriptionally resemble luminal B breast cancer (16–18). This well-established model features activation of major oncogenic signaling pathways implicated in human breast cancer, including the PI3K-mTOR and Ras-MAPK pathways, among others (19–21). It also follows a well-defined progression through distinct premalignant stages to invasive, metastatic disease that closely mimics human breast cancer

Author contributions: L.L., A.H., H.W.S., and W.J.M. designed research; L.L., B.X., D.Z., V.S.-G., and A.J.N. performed research; W.J.M. contributed new reagents/analytic tools; L.L. and B.X. analyzed data; L.L., B.X., H.W.S., and W.J.M. revise the manuscript; L.M. revised and provided suggestions on the manuscript; and L.L., B.X., L.M., and W.J.M. wrote the paper.

The authors declare no competing interest.

This article is a PNAS Direct Submission.

[1]To whom correspondence may be addressed. Email: william.muller@mcgill.ca.

This article contains supporting information online at https://www.pnas.org/lookup/suppl/doi:10.1073/pnas.2303010120/-/DCSupplemental.

Published August 7, 2023.

progression (22, 23). These features, combined with the ability to study breast cancer progression in the context of a fully intact tissue microenvironment, make GEMMs using PyV mT expression indispensable tools for the study of breast cancer.

We recently showed that Ezh2 function is required for metastasis in PyV mT-driven GEMMs due to its repression of an antimetastatic, FOXC1-dependent transcriptional program (24). While this study focused on the role of Ezh2 in the metastatic setting, we also found that ablation of Ezh2 impeded tumorigenesis in GEMMs of both luminal B and HER2 (human epidermal growth factor 2)-positive breast cancer (24, 25). In the study presented here, we investigated the role of Ezh2 in promoting early progression in luminal B models by combining in vivo analysis of an inducible model featuring transcriptionally coupled expression of PyV mT and Cre recombinase (referred to as the MIC model) (23) and in vitro organotypic cultures derived from it. We found that conditional gene targeting of *Ezh2* perturbed the transcriptome in this model, with transcriptional activation of pathways regulating Wnt signaling and inactivation of mTORC1 signaling. We demonstrated that repression of the Wnt pathway inhibitor *Sfrp1* (secreted frizzled-related protein 1) by Ezh2 methyltransferase function disrupts epithelial polarity by activating the Wnt signaling pathway and that SFRP1 expression correlates with a better prognosis in luminal B breast cancer patients. In addition, we observed that the tumor suppressor Phosphatase and tensin homologue deleted on chromosome ten (Pten) is derepressed upon *Ezh2* inhibition, resulting in mTORC1 inhibition in *Ezh2* deficient mammary glands. Collectively, these data argue that Ezh2 activity regulates cell polarity and proliferation by integrating Wnt and mTORC1 signaling, facilitating tumor progression in this model of luminal B breast cancer.

Results

Ablation of *Ezh2* in Mammary Epithelial Cells Impairs Mammary Tumor Initiation. To evaluate the role of *Ezh2* in early mammary tumor progression, we crossed a conditional *Ezh2* knockout strain ($Ezh2^{fl/fl}$) (26) with MMTV-rtTA (27) and the PyVmT-IRES-CRE (MIC) transgenic strains, enabling doxycycline-inducible coexpression of PyV mT and Cre and excision of both *Ezh2* conditional alleles specifically in PyV mT-expressing cells (Fig. 1*A*). We confirmed ablation of Ezh2 protein in MIC/$Ezh2^{fl/fl}$ mammary epithelia, while establishing that PyV mT expression was equivalent to wild-type controls (Fig. 1*B*). In control MIC mice, doxycycline administration for 14 d resulted in robust expression of PyV mT and luminal filling in the mammary epithelium, with proliferating PCNA-positive tumor cells (Fig. 1 *C*–*E*) (28). By contrast, genetic ablation of *Ezh2* significantly reduced luminal filling (Fig. 1 *C* and *D*) and epithelial cell proliferation (Fig. 1*E*) compared to *Ezh2*-proficient controls (Fig. 1*D*).

To determine whether loss of Ezh2 function affected epithelial polarity, we used immunofluorescence to analyze the localization of markers of tight junctions (ZO-1) and adherens junctions (E-cadherin). By contrast to the disorganized epithelial structures in Ezh2-proficient PyV mT lesions, which exhibited diffuse staining of these junctional markers, Ezh2-deficient PyV mT lesions retained highly organized adherens and tight junctional complexes, resembling polarized, nontransformed mammary epithelial cells (Fig. 1*F*). Taken together, these data argue that Ezh2 function is required for the efficient initiation of transformation in this GEMM of luminal B breast cancer.

Ezh2 Methyltransferase Activity Is Critical for the Maintenance of the Transformed Phenotype. To directly investigate the impact of epithelial ablation of *Ezh2* on mammary tumor progression, we established an in vitro organoid culture system using primary mammary epithelial cells that recapitulated the early stages of MIC tumor progression (28). After 6 d of organoid culture, both $Ezh2^{wt/wt}$ MIC and $Ezh2^{fl/fl}$ MIC mammary epithelial cells established polarized organotypic structures. Following doxycycline administration, these MIC organoids coexpressed PyV mT and Cre recombinase, leading to excision of both conditional *Ezh2* alleles in $Ezh2^{fl/fl}$ organoids (Fig. 2*A*). We established that 8 d of doxycycline treatment was the optimal induction period required for efficient turnover of the Ezh2 protein in $Ezh2^{fl/fl}$ MIC organoids (*SI Appendix*, Fig. S1 *A* and *B*) without impacting the level of PyV mT expression (*SI Appendix*, Fig. S2*A*). To monitor the impact of *Ezh2* ablation, we measured organoid diameter, proliferative potential (EdU incorporation), and polarity (E-cadherin and ZO-1 expression and localization) (Fig. 2 *B* and *C*). Consistent with the transformation defect observed in vivo, this revealed that genetic ablation of *Ezh2* resulted in smaller organoids with reduced proliferative capacity (Fig. 2*B*) and retention of adherens and tight junctional complexes (Fig. 2*C*). To investigate whether this phenotype reflected loss of the methyltransferase activity of Ezh2, we treated MIC/$Ezh2^{wt/wt}$ organoids with two chemically unrelated Ezh2 methyltransferase inhibitors (GSK126 and EPZ6438) (Fig. 2*D*) and with the non-SAM-competitive inhibitors DZNep, A-395, and MS-177 (*SI Appendix*, Fig. S3*A*). Pharmacological inhibition of Ezh2 in $Ezh2^{wt/wt}$ MIC organoids, using either SAM-competitive or noncompetitive inhibitors, significantly reduced $H3K27me^3$, decreased organoid diameter and cellular proliferation, and increased the polarization and organization of organoid structures (Fig. 2*E* and *SI Appendix*, Fig. S3*B*), closely phenocopying *Ezh2*-deficient organoids. Together, these observations argue that tumor initiation in this luminal B model is dependent on the methyltransferase activity of Ezh2.

Disruption of Ezh2 Alters the Expression of Genes Involved in Wnt Signaling. To identify Ezh2-regulated genes driving the phenotypes described above, we performed RNA sequencing on samples collected from *Ezh2*-proficient and *Ezh2*-deficient MIC organoids (*SI Appendix*, Fig. S4*A*). Bioinformatic analysis of the transcriptomic data identified 321 genes that were significantly up-regulated and 365 genes with significant downregulation in *Ezh2*-deficient MIC organoids in comparison to their wild-type counterparts (*SI Appendix*, Fig. S4*B*). Since genes that are up-regulated in *Ezh2*-deficient organoids are more likely to include the direct targets of Ezh2-mediated repression, we used gene ontology (GO) analysis to identify regulatory pathways enriched in this gene set. Significant GO terms included those related to regulation of Wnt-activated receptor activity, the F-actin cytoskeleton, and transcriptional activation (Fig. 3*A*). Notably, among the most significantly up-regulated genes in Ezh2-deficient MIC organoids were multiple negative regulators of Wnt signaling, including *Sfrp1*, *Sfrp2*, and *Dkk2* (Fig. 3*B*). To validate these results, we used qRT-PCR to confirm differential expression of mRNAs encoding the Wnt negative regulator *Sfrp1* and Wnt effectors including *Axin2* and *c-Myc* in Ezh2-proficient and deficient organoids (Fig. 3*C*). Ezh2-deficient organoids expressed a significantly higher level of *Sfrp1* transcript and a corresponding decrease in the level of *Axin2* and *c-Myc* compared to their Ezh2-proficient counterparts. Consistent with these genetic ablation studies, treatment of organoids with Ezh2 inhibitors had a similar impact on *Sfrp1*, *c-myc,* and *Axin2* expression (Fig. 3*D*). Because previous studies implicated *Sfrp1* as a target for Ezh2-mediated repression (29), we used chromatin immunoprecipitation (ChIP) with specific antibodies to detect $H3K27me^3$ at the *Sfrp1* promoter in

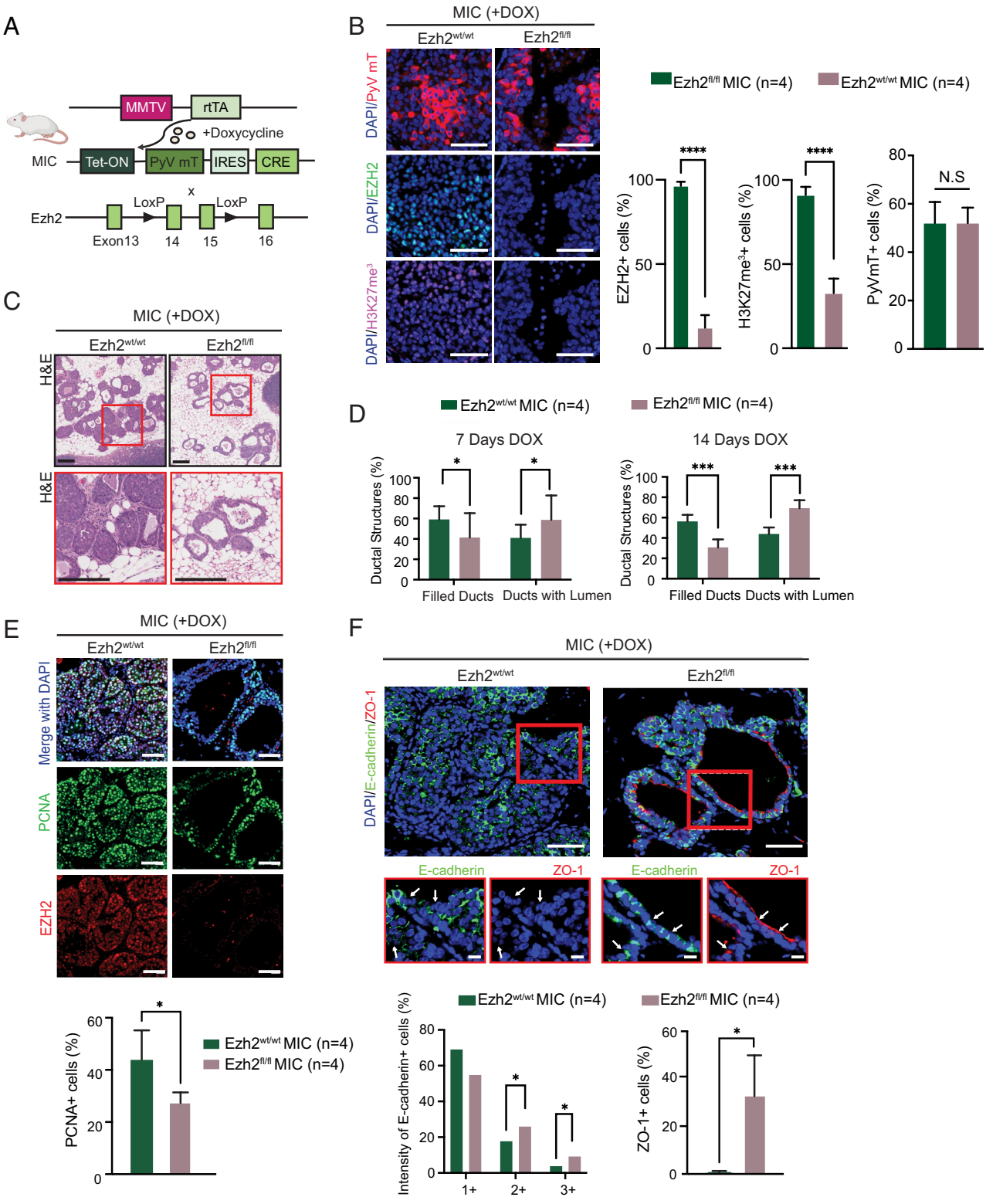

Fig. 1. Genetic loss of *Ezh2* inhibits tumor initiation by reducing proliferation and maintaining cell polarity. (*A*) Schematic of the doxycycline (DOX) inducible transgenic mouse model of PyV mT-IRES-CRE (MIC strain) and the conditional *Ezh2* model. (*B*, *Left*) Immunohistofluorescence (IHF) staining of PyV mT, EZH2, H3K27me^3, and DAPI of MIC wild-type (Ezh2$^{wt/wt}$) and Ezh2$^{fl/fl}$ mammary glands after 2 wk of DOX induction. The scale bar represents 50 μm. (*B*, *Right*) Quantification of PyV mT, EZH2, and H3K27me^3 positive epithelial cells. (*C*) Representative H&E images of Ezh2$^{wt/wt}$ and Ezh2$^{fl/fl}$ mammary glands after 14 d of DOX. (*Upper*) The scale bar represents 50 μm. (*Lower*) 2× zoomed in images of areas outlined in red in C. (*D*) Quantification of ducts with luminal filling or retention at 7 and 14 d of DOX in Ezh2$^{wt/wt}$ and Ezh2$^{fl/fl}$ MIC mice. (*E*, *Upper*) IHF staining of PCNA, EZH2, and DAPI in Ezh2$^{wt/wt}$ and Ezh2$^{fl/fl}$ mammary glands after 2 wk of DOX induction. The scale bar represents 20 μm. (*E*, *Lower*) Quantification of PCNA+ cells. (*F*, *Upper*) IHF staining of E-cadherin, ZO-1, and DAPI in Ezh2$^{wt/wt}$ and Ezh2$^{fl/fl}$ mammary glands after 2 wk of DOX. The scale bar represents 20 μm. (*F*, *Middle*) 2.5× zoomed in images of areas outlined in red in the *Upper*. The scale bar represents 10 μm. (*Lower*) Quantification of E-cadherin intensity and ZO-1 positivity of epithelia. E-cadherin intensity is graded per cell as 1+, 2+, and 3+. All data are presented as mean ± SD, n = 4 mice per genotype, **P* ≤ 0.05, ***P* ≤ 0.01, and ****P* ≤ 0.001, unpaired Student's *t* test. N.S. represents nonsignificance.

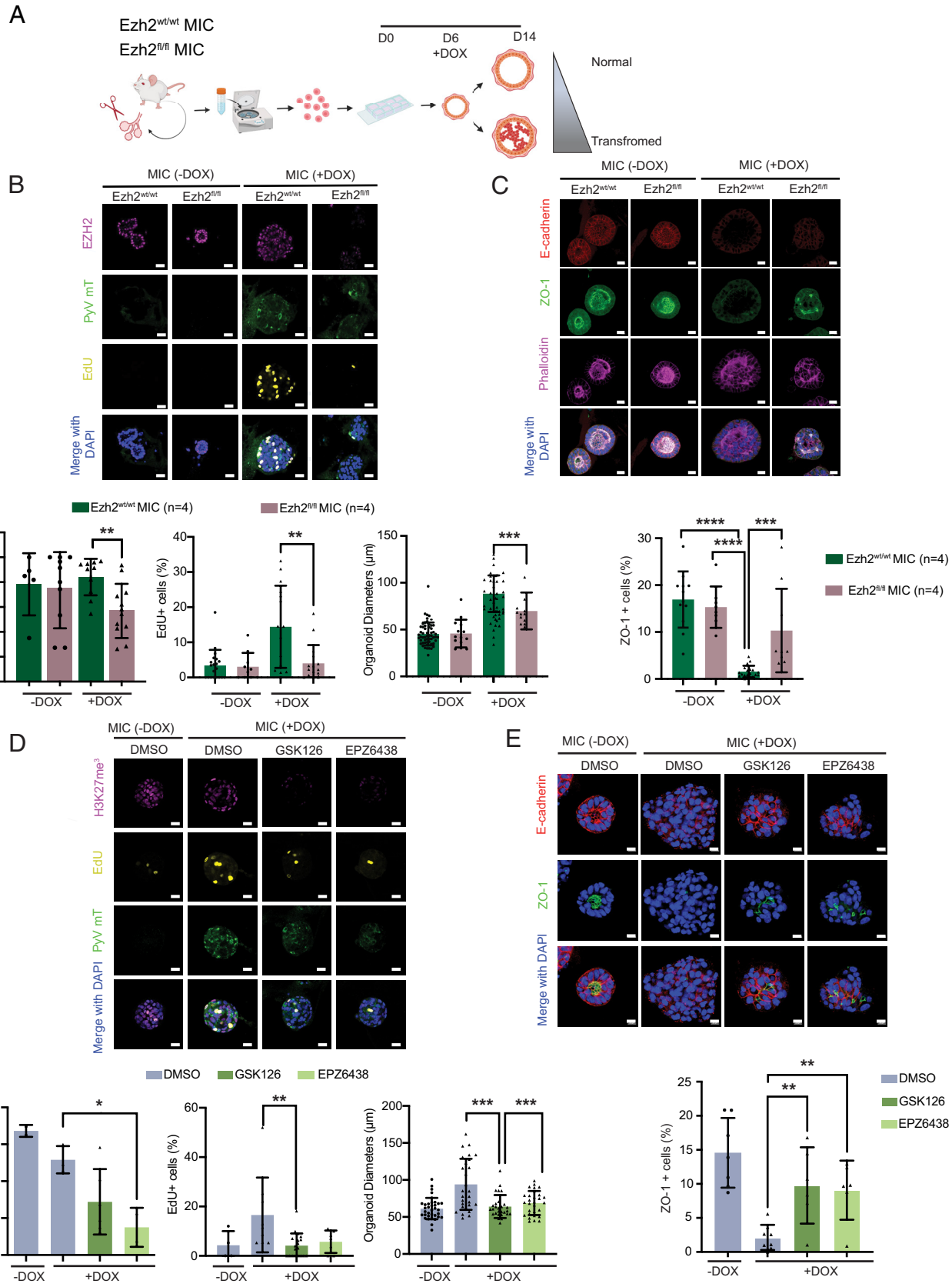

Fig. 2. Genetic or pharmacological inhibition of Ezh2 suppresses proliferation and restores cell polarity. (*A*) Schematic of in vitro 3D organoid model of tumor initiation using mammary epithelial cells derived from Ezh2$^{wt/wt}$ and Ezh2$^{fl/fl}$ MIC mice. (*B*, *Upper*) Immunofluorescence staining (IF) of Ezh2$^{wt/wt}$ and Ezh2$^{fl/fl}$ organoids for EZH2, PyV mT, EdU, and DAPI. The scale bar represents 20 μm. (*B*, *Lower*) Quantification of organoid diameter, EdU incorporation, and EZH2 staining. (*C*, *Upper*) IF staining of Ezh2$^{wt/wt}$ and Ezh2$^{fl/fl}$ organoids for ZO1, E-cadherin, Phalloidin, and DAPI. The scale bar represents 20 μm. (*C*, *Lower*) Quantification of ZO-1-positive cells. (*D*) IF staining (*D*, *Upper*) and quantification (*D*, *Lower*) of H3K27me^3, EdU, and PyV mT and DAPI for Ezh2$^{wt/wt}$ MIC organoids treated with GSK126 (2 nM), EPZ6438 (2 nM), or DMSO, with or without DOX for 8 d. The scale bar represents 20 μm. (*E*, *Upper*) IF staining of E-cadherin and ZO-1 for Ezh2$^{wt/wt}$ MIC organoids treated with GSK126 (2 μM), EPZ6438 (2 μM), or DMSO, with or without DOX for 8 d. (*E*, *Lower*) Quantification of ZO-1 positive cells. The scale bar represents 10 μm. All data are presented as mean ± SD, three mice per genotype, *$P \le 0.05$, **$P \le 0.01$, and ***$P \le 0.001$, unpaired Student's *t* test. N.S. represents nonsignificance.

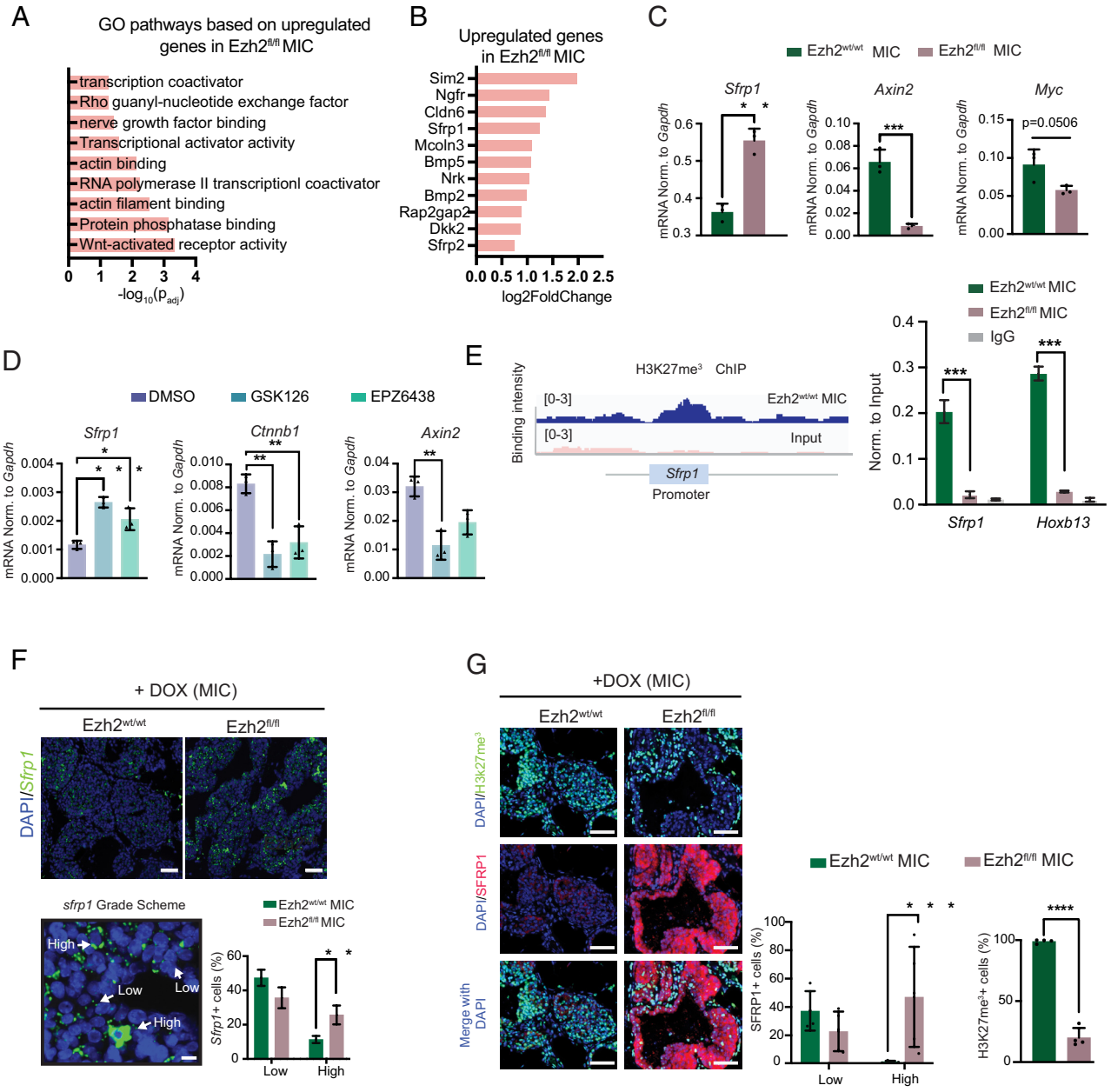

Fig. 3. Loss of Ezh2 function alters Wnt signaling pathways. (*A*) Gene ontology (GO) analysis of up-regulated genes from RNA-Seq. log2FoldChange > 0.5 and $P \leq 0.05$ as a cutoff. (*B*) The most significantly up-regulated genes in Ezh2$^{fl/fl}$ MIC organoids, compared to Ezh2$^{wt/wt}$ MIC organoids, are indicated. (*C*) Quantitative RT-PCR analysis of *Sfrp1Axin2*, and *Myc* (c-Myc) transcript levels in Ezh2$^{wt/wt}$ MIC and Ezh2$^{fl/fl}$ MIC organoids (n = 5 mice pooled per genotype, assay in technical triplicate). (*D*) Quantitative RT-PCR analysis of *Sfrp1Ctnnb1*, and *Axin2* transcript levels in Ezh2$^{wt/wt}$ MIC organoids treated with GSK126 (2 μM), EPZ6438 (2 μM) or DMSO, and DOX for 8 d (pool of n = 4 mice, assays performed in technical triplicate). (*E*, *Left*) Chromatin immunoprecipitation sequencing (ChIP-Seq) analysis of H3K27me^3 in pooled Ezh2$^{wt/wt}$ MIC (n = 8) organoids after 8 d of DOX induction with input control. The image shows H3K27me^3 binding intensity at the *Sfrp1* promoter. (*E*, *Right*) H3K27me^3 ChIP/QRT-PCR analysis of the *Sfrp1* and *Hoxb13* promoters in Ezh2$^{wt/wt}$ MIC (n = 5) and Ezh2$^{fl/fl}$ MIC (n = 5) organoids with IgG as a negative control. (*F*) RNAscope in situ hybridization (ISH) to detect *Sfrp1* in Ezh2$^{wt/wt}$ MIC (n = 4) and Ezh2$^{fl/fl}$ MIC (n = 4) mammary glands after 2 wk of DOX induction. The scale bar represents 50 μm. The grading scheme shows examples of cells with low and high *Sfrp1* transcript levels. (*G*, *Left*) IHF analysis of SFRP1 and H3K27me^3 in Ezh2$^{wt/wt}$ MIC (n = 4) and Ezh2$^{fl/fl}$ MIC (n = 4) mammary glands after 2 wk of DOX induction. The scale bar represents 100 μm. (*G*, *Right*) Quantification of H3K27me^3+ nuclei and epithelial cells with low or high SFRP1 protein levels. All data are mean ± SD. ***$P \leq 0.001$ and ****$P \leq 0.0001$, two-tailed Student's *t* test.

noninduced and induced MIC organoids. This revealed that the induction of PyV mT expression resulted in robust deposition of this repressive chromatin mark on the *Sfrp1* promoter, with significant enrichment over baseline levels observed under noninduced conditions, comparable to that observed for the well-known PRC2 target gene *Hoxb13* (Fig. 3*E*) and correlating with elevated levels of *Sfrp1* transcript in *Ezh2*-deficient organoids compared to *Ezh2*-proficient counterparts (Fig. 3*D*). Taken together, these data argue that Sfrp1 is a direct transcriptional target of Ezh2 in this model which is epigenetically repressed during tumor progression. The impact of altered Wnt signaling was further evaluated through immunofluorescent staining of c-Myc, which showed a substantial reduction in c-Myc protein levels in *Ezh2*-deficient organoid samples (*SI Appendix*, Fig. S5 *A* and *B*). We also observed significantly down-regulated protein expression of c-Myc and the key Wnt pathway regulator β-catenin in vivo (*SI Appendix*, Fig. S5*C*).

Ezh2-Dependent Silencing of SFRP1 Plays a Key Role in the Initiation of Mammary Tumorigenesis. Whereas the above studies focused on MIC organoids, we next validated these observations in primary mammary tissues from Ezh2-proficient and deficient

MIC mice. Using RNA fluorescent in situ hybridization (FISH) analysis, we showed that the *Sfrp1* transcript was dramatically elevated in Ezh2-deficient hyperplasias compared to wild-type controls (Fig. 3*F*). Accordingly, we showed that Ezh2-deficient hyperplasias also expressed elevated levels of Sfrp1 protein compared to Ezh2-proficient controls, which correlated with loss of H3K27me^3 in mammary epithelial cells (Fig. 3*G*). These data argue that *Sfrp1* is a critical target of Ezh2-mediated transcriptional repression in mammary epithelial cells in vivo.

To determine the involvement of *Sfrp1* transcriptional repression in regulation of the transformed phenotype, we used a CRISPR/Cas9-based gene editing approach to genetically ablate *Sfrp1* in Ezh2-proficient and deficient organoids. Using both Sanger sequencing (Fig. 4*A*) and immunofluorescence with Sfrp1-specific antibodies (Fig. 4*B*), we validated successful targeting of the *Sfrp1* allele. While loss of expression of Sfrp1 in Ezh2-deficient organoids did not alter cellular proliferation (*SI Appendix*, Fig. S6*A*), immunostaining of junctional markers such as ZO-1 indicated that loss of Sfrp1 disrupted cellular polarity (Fig. 4*C*), accounting for the increased organoid diameter (*SI Appendix*, Fig. S6*A*). These data argue that Sfrp1 plays a key role in modulating cell polarity, a key hallmark of cellular transformation (30) that is regulated by Wnt signaling pathways during mammary development and carcinogenesis (31, 32).

We confirmed the role of Wnt1 signaling in disrupting epithelial cell polarity during PyV mT-driven tumor initiation by treating doxycycline-induced Ezh2-proficient and deficient MIC organoids with a Wnt pathway inhibitor (IWP-2) or vehicle control. This showed that inhibition of Wnt signaling restored the polarized phenotype in PyV mT-expressing mammary epithelial cells (Fig. 4 *D* and *E*). Collectively, these data argue that Sfrp1 and Wnt signaling play opposing roles in regulating epithelial polarity during mammary epithelial transformation. Consistent with these findings, analyses of TCGA breast cancer datasets revealed that expression of *SFRP1* was inversely correlated with *EZH2* expression in multiple breast cancer subtypes, with the notable exception of the basal breast cancer intrinsic subtype (*SI Appendix*, Fig. S7*A*). Of direct relevance to our studies using the MIC GEMM of luminal B breast cancer, *SFRP1* expression correlated with good patient outcome in luminal B breast cancer patients (*SI Appendix*, Fig. S7*B*).

A

Relative contribution of each sequence		
Indel	Frequency	Sfrp1 -/- Sequence
0(wt)	0.06	GTCGGGCGCAGCGCGCGGGGTCGCG|GCGGGGCCGCCTCGGGAAGTGCTGCTGGCGTTG
-1	0.76	GTCGGGCGCAGCGCGCGGGGTCGCG|-CGGGGCCGCCTCGGGAAGTGCTGCTGGCGTTG
-14	0.01	GTCGGGCGCAGCGCGCGGGGTCGCG|----------GGAAGTGCTGCTGGCGTTGGCCGCC
-18	0.01	GTCGGGCGCAGCGCGCGGGGTCGCG|----------GTGCTGCTGGCGTTGGCCGCCGC
-39	0.01	GTCGGG----------|----------GCTGCTGGCGTTGGCCGCCGCTCTGCTGGCCT

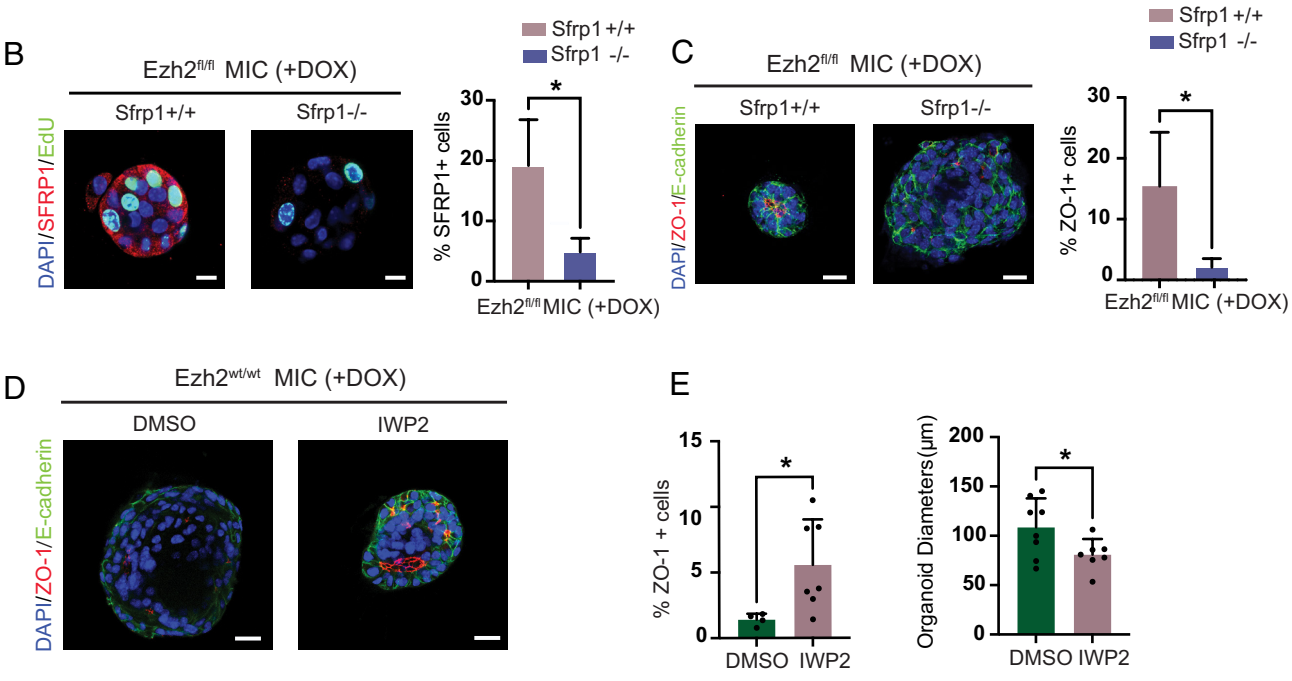

Fig. 4. Sfrp1 impedes tumor initiation in Ezh2-deficient mammary epithelium. (*A*) Percentage of Indels (insertions and deletions) at the *Sfrp1* locus in genomic DNA from CRISPR-Cas9-edited or nonedited Ezh2$^{fl/fl}$ organoids grown for 8 d (n = 3 mice pooled). (*B*) IF staining (*Left*) and quantification (*Right*) of Sfrp1 in Ezh2$^{fl/fl}$ MIC organoids with or without *Sfrp1* deletion via CRISPR-mediated genome editing. The scale bar represents 10 µm. Mean ± SD, **P* ≤ 0.05. (*C*) IF staining (*Left*) and analysis (*Right*) of cell junction markers ZO-1 and E-cadherin. The scale bar represents 20 µm. Quantification of ZO-1+ cells, mean ± SD, **P* ≤ 0.05 using Student's two-tailed *t* test. (*D*) Immunofluorescence staining of ZO-1 and E-cadherin using Ezh2$^{wt/wt}$ organoids treated with 20 nM IWP-2 or DMSO. The scale bar represents 20 µm. (*E*) Quantification of ZO-1 expression and organoid diameters. All quantitative data are mean ± SD. **P* ≤ 0.05, unpaired Student's *t* test.

Indeed, loss of *SFRP1* expression in human breast cancer patients has been noted during the transition of ductal carcinoma in situ (DCIS) to the invasive phenotype (33, 34). Together, these data argue that loss of SFRP1 is an early event in breast cancer progression.

Loss of Ezh2 Impairs mTORC1 Signaling in a GEMM of Luminal B Breast Cancer. GO analysis of genes significantly down-regulated in our transcriptomic analysis of *Ezh2*-deficient and proficient MIC organoids revealed that loss of Ezh2 function reduced the expression of critical ribosomal genes such as *Rpl35* and *Rpl23a* (Fig. 5 *A* and *B*) which are regulated by the mTORC1 signaling pathway, a master regulator of ribosome biogenesis including the transcription and processing of mRNAs encoding ribosomal proteins (35, 36)**.** To investigate the effects of Ezh2 ablation on mTORC1 activity, we evaluated the phosphorylation of ribosomal protein S6 (p-S6) and of eIF4E binding protein 1 (p-4EBP1), which are well-established readouts of mTORC1 signaling (37–39). We observed significant decreases in p-4EBP1 and p-S6 levels in *Ezh2*-deficient organoid samples (*SI Appendix*, Fig. S8 *A* and *B*). These findings suggest that downregulation of mTORC1 signaling is a potential cause of the decreased cell proliferation observed in the absence of Ezh2. Indeed, our previous work demonstrated that increased mTORC1 activation is crucial for the early stages of mammary tumor initiation, where loss of activity results in severe proliferation defects (40). We validated findings from the transcriptomic dataset by using quantitative RT-PCR to show that key ribosomal genes were significantly down-regulated in *Ezh2*-deficient organoids in comparison to their wild-type counterparts (Fig. 5*C*). To directly assess the consequences of mTORC1 inhibition on organoid formation, we targeted mTORC1 pharmacologically using the inhibitors Rapamycin and Torin-1, both of which restored cellular polarity and decreased organoid size, phenocopying the genetic ablation of Ezh2 in the organoid system (Fig. 5 *D* and *E*). We observed similar effects using GDC-0941, an inhibitor of PI3K which acts upstream of mTORC1 (*SI Appendix*, Fig. S9 *A–F*). Both mTORC1 inhibitors and the PI3K inhibitor reduced the residual activity of mTORC1 in Ezh2-deficient MIC organoids, leading to a further suppression of proliferation and organoid diameter relative to wild-type controls. However, they did not have a significant further effect on cell polarity, consistent with the association of this aspect of the Ezh2-deficient phenotype with effects on Wnt signaling (Fig. 4).

To validate effects on mTORC1 signaling in the absence of Ezh2 in vivo, we examined p-S6 and p-4EBP1 levels in mammary gland samples from $Ezh2^{fl/fl}$ MIC and $Ezh2^{wt/wt}$ MIC mice induced for 2 wk with doxycycline. This analysis confirmed that loss of Ezh2 in the mammary epithelium blocks the activation of mTORC1 by PyV mT signaling in vivo (Fig. 5*F*). Because the tumor suppressor *PTEN*, a key negative regulator of mTORC1 that functions by opposing the activity of PI3K, is a direct target of EZH2-dependent transcriptional repression in basal breast cancer (41), we investigated whether reactivation of Pten expression is a potential mechanism linking Ezh2 loss with mTORC1 downregulation in the MIC model. While we detected a robust restoration of Pten protein expression in the mammary epithelia of 2-wk doxycycline-induced $Ezh2^{fl/fl}$ MIC mice compared to $Ezh2^{wt/wt}$ controls, ChIP analysis revealed that *Pten* is not a direct target of Ezh2-mediated repression in this luminal B GEMM (*SI Appendix*, Fig. S9*G*). Therefore, while activation of Pten expression is likely to contribute to the observed phenotypes in *Ezh2*-deficient MIC mammary epithelial cells, the effect of *Ezh2* deletion on Pten is indirect. Supporting the relevance of our observations to human breast cancer, we identified a significant inverse correlation between the expression of the *PTEN* and *EZH2* mRNAs in breast cancer patients using TCGA RNA-Seq data (*SI Appendix*, Fig. S9*H*).

Discussion

The genetic and epigenetic events underlying breast cancer initiation are poorly understood. In this study, we focused on the role of the key histone modifier and transcriptional repressor PRC2 in the initiation of luminal B breast cancer, an aggressive form of the disease where there are unmet clinical needs for more effective therapies that can improve patient outcomes (42). Our strategy was based on our previous findings that targeting the major catalytic subunit of PRC2, the H3K27 methyltransferase Ezh2, significantly delayed tumor onset and blocked metastasis in a PyV mT-expressing GEMM mimicking the luminal B subtype (24). Combining multiple in vitro and in vivo analyses, we found that targeting Ezh2 in organoids and in hyperplastic lesions in the mammary epithelium in vivo reduced proliferative capacity and promoted the retention of a polarized epithelial phenotype. Taken together, these data indicate that Ezh2 plays a critical role in tumor initiation in this GEMM of luminal B breast cancer (Fig. 6). These findings are in contrast to those of studies using mammary epithelial *Ezh2* gene targeting in a *Brca1*-deficient GEMM, where loss of Ezh2 had little impact on tumor initiation (43). However, unlike the MIC model, where loss of Ezh2 resulted in a profound loss of $H3K27me^3$ (Figs. 1*B* and 3*G*) (24), the BRCA1 deficient tumors retained this repressive chromatin mark (43) indicating a potential functional redundancy of Ezh1 for which there is no evidence in our model. In addition to the *Brca1* GEMM, loss of Ezh2 function had little impact on mammary tumor formation in a Notch-driven GEMM of breast cancer (9). Consistent with these triple-negative breast cancer (TNBC) GEMMs, we previously showed that inhibition of Ezh2 had little impact on tumor cell growth and survival in TNBC (24). However, like the MIC model, genetic loss of *Ezh2* in GEMMs mimicking the HER2-positive breast cancer subtype blocked tumor initiation due to inhibition of tumor cell proliferation (25). The observations of the present study, in the context of published work, are therefore consistent with the known context dependency of the oncogenic function of Ezh2/PRC2 (44, 45), whereby functional requirements for PRC2 during breast cancer progression are highly dependent on molecular subtype.

Transcriptomic and biochemical analysis of *Ezh2*-proficient and deficient organoids revealed that genes involved in the Wnt and mTORC1 signaling pathways were profoundly affected by the loss of *Ezh2*. We validated *Sfrp1*, a potent inhibitor of Wnt signaling, as a direct target of Ezh2-mediated repression (Fig. 3 *C* and *D*) and showed that CRISPR-Cas9-mediated ablation of *Sfrp1* partially restored the transformed phenotype in *Ezh2* deficient MIC organoids by disrupting epithelial polarity (Fig. 4 *B* and *C* and *SI Appendix*, Fig. S6*A*). The incomplete nature of this phenotypic rescue likely reflects the fact that other inhibitors of Wnt1 signaling, including Sfrp2 and Dkk1, are still expressed in the absence of *Sfrp1* (Fig. 3*B*). The involvement of Ezh2 in Wnt-dependent signaling has been documented in other tissue contexts. For example, EZH2 has been demonstrated to cotarget β-catenin-responsive genes in Wnt10a-expressing mammary tumors, leading to a chemo-resistant phenotype (46). In colon cancer, EZH2 and Wnt/β-catenin expression are involved in tumor progression (47). Emerging evidence has demonstrated the importance of Wnt signaling in the PyV mT GEMM (48–50), and the potential involvement of Wnt-dependent pathways in luminal B breast cancer progression is an interesting area for further study.

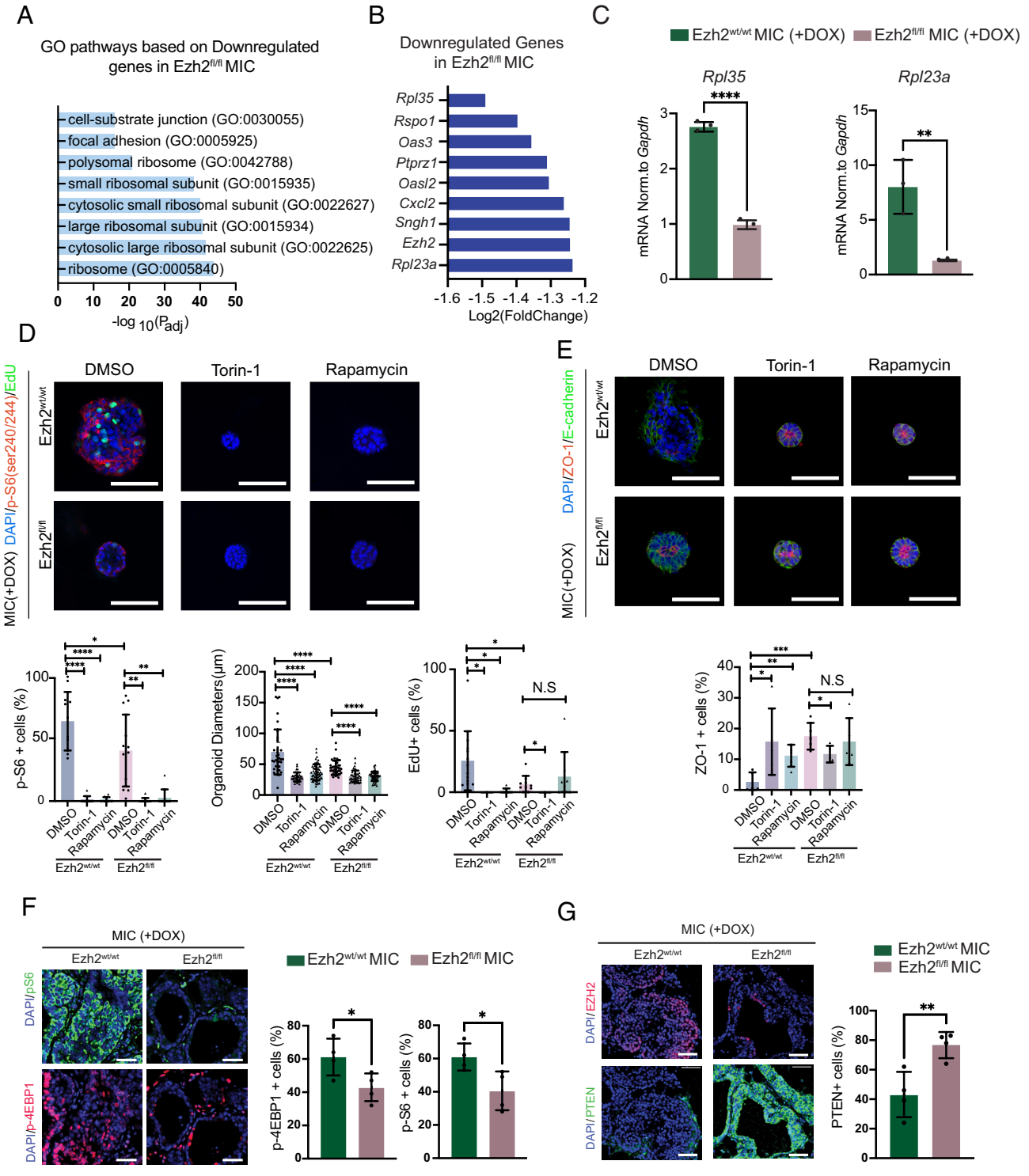

Fig. 5. Suppression of mTOR signaling pathway through PTEN derepression by EZH2. (*A*) GO analysis of genes down-regulated in Ezh2$^{fl/fl}$ MIC organoids compared to Ezh2$^{wt/wt}$ MIC organoids, with cutoffs of log2FoldChange < −0.5 and $P \le 0.05$. (*B*) The most significantly down-regulated genes in Ezh2$^{fl/fl}$ MIC organoids, compared to Ezh2$^{wt/wt}$ MIC organoids, are indicated. (*C*) Quantitative RT-PCR validation of *Rpl35* and *Rpl32* in MIC organoids after 8 d of DOX induction (n = 3 mice pooled for each group, assays performed in technical triplicate). Mean ± SD. (*D*, *Upper*) IF staining and analysis of p-S6 (ser240/244) in Ezh2$^{wt/wt}$ and Ezh2$^{fl/fl}$ MIC organoids induced with DOX for 8 d and treated with the mTOR inhibitors Torin-1 (250 nM) or Rapamycin (100 nM) or vehicle (DMSO). The scale bar represents 50 μm. (*D*, *Lower*) Quantification of p-S6 staining and organoid diameter. (*E*, *Left*) IF staining of E-cadherin and ZO-1 on Ezh2$^{wt/wt}$ and Ezh2$^{fl/fl}$ organoids treated as in *D*. The scale bar represents 50 μm. (*E*, *Right*) Quantification of ZO-1+ cells. (*F*, *Left*) IHF staining of p-S6 (Ser240/244) and p-4EBP1(Thr37/46) in Ezh2$^{wt/wt}$ MIC (n = 4) and Ezh2$^{fl/fl}$ MIC (n = 4) mammary glands. The scale bar represents 20 μm. (*Right*) Quantification of p-S6(Ser240/244) cytoplasmic staining and p-4EBP1(Thr37/46) nuclear staining. (*G*) IHF staining (*G*, *Left*) and analysis (*G*, *Right*) of Pten and Ezh2. The scale bar represents 20 μm. Quantification of Pten+ cells (n = 4 per group). All quantitative data are mean ± SD. *$P \le 0.05$, **$P \le 0.01$, ***$P \le 0.001$, and ****$P \le 0.0001$, two-tailed Student's *t* test.

In agreement with the involvement of Wnt/β-catenin signaling, we have shown that administration of Wnt signaling inhibitors alone can partially phenocopy the Ezh2-deficient phenotype (Fig. 4*D*), arguing that Ezh2 and Wnt act cooperatively to promote malignant transformation in models of luminal B breast cancer.

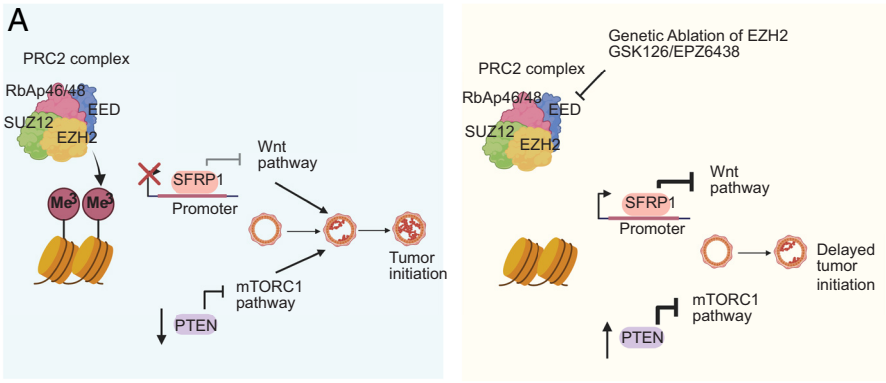

Fig. 6. EZH2 promotes mammary tumor initiation through epigenetic regulation of the Wnt and mTORC1 signaling pathways (*A*) Schematic of proposed mechanism illustrating the impact of EZH2 on the initiation of luminal B mammary tumors.

In contrast to its effects on Wnt signaling, regulation of mTORC1 by Ezh2 appears to involve indirect mechanisms. We identified a dramatic reduction in the expression of genes encoding ribosomal proteins (e.g., Rpl35 and Rpl23a) in Ezh2-deficient MIC organoids (Fig. 5 *A*–*C*) that correlated with significant downregulation of mTORC1 phosphorylation targets 4EBP1 and rpS6 in Ezh2-deficient MIC organoids and primary tissues (Fig. 5 *D*–*G* and *SI Appendix*, Fig. S8 *A* and *B*). Given the well-established roles of these ribosomal proteins and of mTORC1, these changes would be predicted to have a major effect on mRNA translation (35, 51) that could compromise the proliferation and growth of emerging mammary tumor cells. Although previous studies have demonstrated that mTORC1 activity promotes the translation of *Ezh2* and enhances the production of the methyl donor S-adenosylmethionine (SAM), the cosubstrate of Ezh2 (25, 52), how loss of Ezh2 impacts mTORC1 signaling in breast cancer is unclear. Our data suggest that upregulation of Pten, which potently suppresses mTORC1 activation by opposing the activity of the PI3K-Akt signaling cascade, could be involved (Fig. 5*G*). However, although EZH2 is known to target the *PTEN* promoter during glioblastoma development (53), we could not detect H3K27me^3 within the *Pten* promoter in our MIC system, arguing that the induction of Pten expression in Ezh2-deficient mammary epithelial cells is indirect. Examples of such indirect mechanisms regulating *PTEN* expression involving coordinated NOTCH and EZH2 activity have been documented (41). Other possibilities include the involvement of long noncoding RNAs (lncRNAs). For example, in prostate cancer, EZH2-dependent regulation of the lncRNA SNHG1 regulates Wnt/β-Catenin and PI3K/AKT/mTOR signaling (54). Assessment of these possible regulatory interactions in breast cancer represents another promising avenue for future investigation.

Overall, our study supports the concept that Ezh2 is a master regulator of multiple oncogene-coupled signaling pathways during the tumor initiation phase in models of luminal B breast cancer, impacting on mRNA translation, cell proliferation, and cell polarity. Consistent with our findings, the expression of EZH2 targets such as *SFRP1* is associated with better clinical outcome in luminal B breast cancer. These data are consistent with the therapeutic potential of targeting EZH2 in some subtypes of breast cancer. Further characterization of EZH2-dependent transcriptional networks responsible for tumor initiation and progression in defined molecular subtypes may also allow the design of therapeutic strategies targeting the key nodes of EZH2 signaling in breast cancer.

Materials and Methods

Experimental Animal Models. The MMTV-rtTA, Tet-ON-PyVmT-IRES-CRE, and conditional *Ezh2* knockout mouse strains used in this study were described previously (23, 27) and maintained on a pure FVB/N genetic background. Offspring carrying both the MMTV-rtTA and the Tet-ON-PyVmT-IRES-CRE transgenes, herein referred to as the MIC strain, were provided with water supplemented with Doxycycline (Wisent) at 8 to 12 wk old. All studies involving mice were approved by the McGill University Animal Care Committee and Facility Animal Care Committee and were fully compliant with institutional and Canadian Council on Animal Care ethical guidelines.

In Vitro Tissue Culture of Mammary Organoids. Epithelial cells were harvested from the mammary glands of 8 to 12-wk-old MIC mice and grown as organoids as described previously (28). Roughly 10,000 mammary epithelial cells were cultured in eight-well chambers in the organotypic medium consisted of Epicult-B mouse medium (Stem Cell Technologies, 05610), knockout serum replacement (Gibco, 10828010), penicillin/streptomycin, 10 ng/mL EGF, 25 μg/mL insulin (Sigma, 10156), and 1 μg/mL hydrocorticone for 6 d to allow formation of acinar structures. Subsequently, doxycycline was added to growth media either in the presence or absence of drug treatments for 8 d, with media changes every 48 h. The following inhibitors, along with their working doses, were used: GSK-126 (MedChem Express, Cat#HY-13470, 2 μM), EPZ6438 (MedChem Express, Cat#13803, 2 μM), Torin-1 (Selleckchem, Cat#S2827, 250 nM), Rapamycin (MedChem Express, Cat#HY-10219, 100 nM), IWP-2 (STEMCELL Technologies, Cat#721220, 20 nM), MS-177 (MedChem Express, Cat#HY-148333, 5 μM), A-395 (MedChem Express, Cat#HY-101512, 2.5 μM), 3-Deazaneplanocin A hydrochloride (DZNep) (MedChem Express, Cat#HY-10442, 2 μM), and Pictilisib (GDC-0941) (MedChem Express, Cat#HY-50094, 5 μM).

Immunofluorescence and Immunohistochemistry. For immunofluorescence, organoids were grown in eight-well chambers and incubated with EdU for 4 h prior to cell fixation with 4% paraformaldehyde. Samples were permeabilized with PBS + 0.2% Triton-X100 for 10 min, blocked with PBS + 0.2%Triton-X100 + 0.05% Tween-20 + 2% BSA for 30 min, and incubated with primary and secondary antibodies at room temperature. Antibodies are described in *SI Appendix*, Table S1. EdU incorporation assays were performed using the Click-it EdU imaging kit (ThermoFisher, C10338) according to the manufacturer's instructions. Nuclei were visualized by staining samples with DAPI (Dihydrochloride, ThermoFisher, D1306, 2 μg/mL) prior to being mounted onto a glass slide for imaging using a Zeiss LSM800 confocal microscope. Organoid sizes were quantified by measuring the diameter of 20 to 40 individual organoids per condition using ZEN software, and fluorescent staining was analyzed by using Halo software (Indica Labs).

Immunofluorescent staining of tissue was based on protocols described previously (24). Immunofluorescence images were acquired using an Axio scanner (Zeiss) and analyzed by using HALO software (Indica Labs).

Immunoblotting. Mammary organoids were collected after 8 d of doxycycline induction and lysed in RIPA buffer (150 mM sodium chloride, 50 Mm Tris–HCL pH7.4, 2 mM EDTA, 10 mM sodium fluoride (Sigma, S7920), 10 mM sodium

pyrophosphate, 1% sodium deoxycholate, 1% Nonidet P-40, 1 mM sodium orthovanadate, 1 mM PMSF, 10 mM sodium fluoride, 25 mM β-glycerophosphate (Sigma, G5422), 10 μg/μL leupeptin, and 10 μg/μL aprotinin). Immunoblotting was based on protocols described previously (40). Antibodies are described in *SI Appendix*, Table S1.

Flow Cytometry. Mammary organoids were collected and trypsinized with 0.05%-EDTA trypsin (Wisent) into a single-cell suspension prior to passage through a 70-μm strainer for flow cytometry analysis. One million cells were treated with TruStain FcX blocking solution (BioLegend, 101320) for 10 min prior to incubation with primary antibody for 30 min on ice. Subsequently, the stained cells were fixed at RT for 15 min using BD Cytofix Fixation buffer (BD Bioscience, 554655) and washed with BD Perm/Wash™ buffer (BD Bioscience, 554723) prior to being treated with the DNA dye 7-AAD (7-amino-actinomycin D) (BioLegend, 420404). The stained cells were visualized by flow cytometry using a BD LSR Fortessa flow cytometer (BD Biosciences, San Jose, CA). A minimum of 250,000 events were acquired per experiment in slow rate mode. Data analysis was performed with FlowJo software (Ashland, OR, USA). Cell debris and aggregates were excluded from the analysis using SSC-H/ SSC-W, and 7-AAD-A/ 7-AAD-W parameters.

RNA/DNA Extraction, RNAseq Processing, and Bioinformatics Analysis. Mammary organoids were collected after 8 d of doxycycline induction and lysed for RNA purification using a commercial total RNA Purification kit (Favorgene, Cat# FATRK 011-2). The purified RNA was quantified using a Qubit 2.0 Fluorometer (Life Technologies, CA, USA) according to the manufacturer's instructions and submitted for RNAseq analysis via the Illumina NovaSeq platform offered by Novogene. RNA was sequenced and analyzed as previously described (10). Raw RNAseq data were processed by the Bioinformatics Core at the GCI, McGill University. Differential expression analysis was performed using the DEGseq2 R package (2_1.6.3), with *P* values adjusted using Benjamini and Hochberg's method. Genes with adjusted *P* values of less than 0.05 were considered to be differentially expressed. Ingenuity Pathway Analysis software (RRID:SCR_008653) was used to perform Gene Ontology (GO) analysis.

RT-PCR Analysis. cDNA was generated with the TranScript All-in-One cDNA Synthesis SuperMix kit (CivicBio, AT341) according to the manufacturer's instructions, and quantitative RT-PCR was performed using SYBR Green Master Mix (Roche) where data were normalized to *Gapdh*. Primer sequences are described in *SI Appendix*, Table S2.

RNA In Situ Hybridization. RNA in situ hybridization detecting mouse *Sfrp1* was conducted using RNAcope Probe-Mm-Sfrp1 (Advanced Cell Diagnostics, Cat#404981) and visualized with BaseScope Duplex Detection Reagent (Advanced Cell Diagnostics, Cat#323800), according to the manufacturer's instructions.

Chromatin Immunoprecipitation. ChIP assays were performed using a SimpleChIP Enzymatic Chromatin IP kit (Cell Signaling, Cat#9003) based on the manufacturer's instructions. Ezh2$^{wt/wt}$ MIC organoids were treated with doxycycline for 8 d prior to fixation and cross-linking with 1% formaldehyde for 10 min. Chromatin fragmentation was achieved by micrococcal nuclease treatment, and modified histones were immunoprecipitated using an H3K27me^3 antibody (Cell Signaling, Cat#9733) and ChIP Grade magnetic beads. The DNA was isolated with a commercial DNA purification spin column (Cell Signaling Cat#14209S) following cross-link removal and submitted to Novogene for ChIP-seq analysis.

CRISPR-Cas9-Directed Knockout of *Sfrp1*. CRISPR-mediated knockout of *Sfrp1* was achieved using the Gene Knockout Kit v2 - mouse – *Sfrp1* (Synthego). Mammary epithelial cells were isolated from Ezh2$^{wt/wt}$ MIC and Ezh2$^{fl/fl}$ MIC mice and cultured in suspension for 24 h, and 3×10^6 cells per genotype were electroporated using the Mix Lonza Amaxa Cell line Nucleofector Kit (Lonza: VPI-1005). Stock solutions of 100 μM (100 pmol/μL) sgRNA were prepared using nuclease-free buffer (1XTE buffer). Ribonucleoprotein (RNP) complexes were formed by mixing a 9:1 sgRNA to Cas9 2NLS (GenScript, Z03393) ratio in Nucleofector Solution with Supplement (4.5:1, Lonza) at room temperature for 10 min. Fifty microliters of reagent containing RNP complex was added to 3×10^6 cells into Nucleocuvette vessel, and the program T-020 from the Lonza Nucleofector device was applied. Five hundred microliters of pre-equilibrated culture medium was added immediately to the cuvette, and the sample was gently transferred into a poly-Hema coated plate with cell culture medium. Half of the obtained cells were grown on eight-well plates with Geltrex (Gibco, A1413201) for 6 d prior to 8 d of doxycycline induction. The remaining cells were grown in suspension for 8 d under doxycycline induction prior to being pelleted for DNA extraction with an All Prep DNA/RNA/Protein mini kit (Qiagen, 80004), and the *Sfrp1* gene was sequenced to detect small insertion or deletion mutations via Sanger sequencing. sgRNAs are described in *SI Appendix*, Table S3.

Quantification and Statistical Analysis. All statistical analysis and quantification were performed using Graphpad Prism version 9. Two-tailed Student's *t* tests were used to evaluate significance, $*P < 0.5$, $**P < 0.01$, $***P < 0.001$, and $****P < 0.0001$. Kaplan–Meier Analysis was done through KM-plotter (55).

Data, Materials, and Software Availability. Transcriptomic data (RNA-Seq) and ChIP-seq data have been deposited at the GEO repository, with the accession number (GSE235147) (56). All study data are included in the article and/or *SI Appendix*.

ACKNOWLEDGMENTS. We would like to acknowledge Cynthia Lavoie, the Goodman Cancer Institute Histology Core, Alain Pacis from the Goodman Cancer Institute Bioinformatics Technology Platform, and the Comparative Medicine and Animal Resources Center for their technical support. Figs. 2*A* and 6 were generated using tools provided by Biorender.com. We would like to thank Dr. Tung Bui, Sherif Attala, Hailey Proud, Yu Gu, and Ipshita Nandi for their comments and editorial suggestions. This work was funded by a Canadian Cancer Society Research Institute Impact Grant (Grant number: 706679). W.J.M. was supported by a Tier 1 Canada Research Chair in Molecular Oncology (Grant number: CRC-2015-00301x-216779).

Author affiliations: [a]Rosalind and Morris Goodman Cancer Research Institute, McGill University, Montreal, QC H3A 1A3, Canada; [b]Department of Biochemistry, McGill University, Montreal, QC H3A 1A3, Canada; [c]Department of Medicine, McGill University, Montreal, QC H3A 1A3, Canada; and [d]Department of Oncology, McGill University, Montreal, QC H3A0G4, Canada

1. G. Turashvili, E. Brogi, Tumor heterogeneity in breast cancer. *Front. Med. (Lausanne)* **4**, 227 (2017).
2. J. E. Visvader, Cells of origin in cancer. *Nature* **469**, 314–322 (2011).
3. A. Laugesen, J. W. Hojfeldt, K. Helin, Molecular mechanisms directing PRC2 recruitment and H3K27 methylation. *Mol. Cell* **74**, 8–18 (2019).
4. Y. Yao *et al.*, Downregulation of enhancer of zeste homolog 2 (EZH2) is essential for the induction of autophagy and apoptosis in colorectal cancer cells. *Genes. (Basel)* **7**, 83 (2016).
5. Y. Huang, S. Nayak, R. Jankowitz, N. E. Davidson, S. Oesterreich, Epigenetics in breast cancer: What's new? *Breast Cancer Res.* **13**, 225 (2011).
6. J. Jovanovic, J. A. Ronneberg, J. Tost, V. Kristensen, The epigenetics of breast cancer. *Mol. Oncol.* **4**, 242–254 (2010).
7. L. Garcia-Martinez, Y. Zhang, Y. Nakata, H. L. Chan, L. Morey, Epigenetic mechanisms in breast cancer therapy and resistance. *Nat. Commun.* **12**, 1786 (2021).
8. R. Margueron, D. Reinberg, The polycomb complex PRC2 and its mark in life. *Nature* **469**, 343–349 (2011).
9. M. Wassef *et al.*, Impaired PRC2 activity promotes transcriptional instability and favors breast tumorigenesis. *Genes. Dev.* **29**, 2547–2562 (2015).
10. R. Cao *et al.*, Role of histone H3 lysine 27 methylation in Polycomb-group silencing. *Science* **298**, 1039–1043 (2002).
11. I. M. Bachmann *et al.*, EZH2 expression is associated with high proliferation rate and aggressive tumor subgroups in cutaneous melanoma and cancers of the endometrium, prostate, and breast. *J. Clin. Oncol.* **24**, 268–273 (2006).
12. C. G. Kleer *et al.*, EZH2 is a marker of aggressive breast cancer and promotes neoplastic transformation of breast epithelial cells. *Proc. Natl. Acad. Sci. U.S.A.* **100**, 11606–11611 (2003).
13. M. Koppens, M. van Lohuizen, Context-dependent actions of Polycomb repressors in cancer. *Oncogene* **35**, 1341–1352 (2016).
14. K. Holm *et al.*, Global H3K27 trimethylation and EZH2 abundance in breast tumor subtypes. *Mol. Oncol.* **6**, 494–506 (2012).
15. S. T. Lee *et al.*, Context-specific regulation of NF-kappaB target gene expression by EZH2 in breast cancers. *Mol. Cell* **43**, 798–810 (2011).
16. A. D. Pfefferle *et al.*, Transcriptomic classification of genetically engineered mouse models of breast cancer identifies human subtype counterparts. *Genome Biol.* **14**, R125 (2013).
17. S. T. Attalla, T. Taifour, T. Bui, W. Muller, Insights from transgenic mouse models of PyMT induced breast cancer: Recapitulating human breast cancer progression in vivo. *Oncogene* **40**, 475–491 (2021).

18. I. K. Mieczkowska *et al.*, Decreased PRC2 activity supports the survival of basal-like breast cancer cells to cytotoxic treatments. *Cell Death Dis.* **12**, 1118 (2021).
19. S. Attalla, T. Taifour, T. Bui, W. Muller, Insights from transgenic mouse models of PyMT-induced breast cancer: Recapitulating human breast cancer progression in vivo. *Oncogene* **40**, 475–491 (2021).
20. J. Hutchinson, J. Jin, R. D. Cardiff, J. R. Woodgett, W. J. Muller, Activation of Akt (protein kinase B) in mammary epithelium provides a critical cell survival signal required for tumor progression. *Mol. Cell Biol.* **21**, 2203–2212 (2001).
21. J. Ursini-Siegel *et al.*, ShcA signalling is essential for tumour progression in mouse models of human breast cancer. *EMBO J.* **27**, 910–920 (2008).
22. J. E. Maglione *et al.*, Transgenic polyoma middle-T mice model premalignant mammary disease. *Cancer Res.* **61**, 8298–8305 (2001).
23. T. Rao *et al.*, Inducible and coupled expression of the polyomavirus middle T antigen and Cre recombinase in transgenic mice: an in vivo model for synthetic viability in mammary tumour progression. *Breast Cancer Res.* **16**, R11 (2014).
24. A. Hirukawa *et al.*, Targeting EZH2 reactivates a breast cancer subtype-specific anti-metastatic transcriptional program. *Nat. Commun.* **9**, 2547 (2018).
25. H. W. Smith *et al.*, An ErbB2/c-Src axis links bioenergetics with PRC2 translation to drive epigenetic reprogramming and mammary tumorigenesis. *Nat. Commun.* **10**, 2901 (2019).
26. X. Shen *et al.*, EZH1 mediates methylation on histone H3 lysine 27 and complements EZH2 in maintaining stem cell identity and executing pluripotency. *Mol. Cell* **32**, 491–502 (2008).
27. E. J. Gunther *et al.*, A novel doxycycline-inducible system for the transgenic analysis of mammary gland biology. *FASEB J.* **16**, 283–292 (2002).
28. R. Halaoui *et al.*, Progressive polarity loss and luminal collapse disrupt tissue organization in carcinoma. *Genes. Dev.* **31**, 1573–1587 (2017).
29. J. Yu *et al.*, MBD2 and EZH2 regulate the expression of SFRP1 without affecting its methylation status in a colorectal cancer cell line. *Exp. Ther. Med.* **20**, 242 (2020).
30. D. Hanahan, R. A. Weinberg, Hallmarks of cancer: The next generation. *Cell* **144**, 646–674 (2011).
31. X. Xu, M. Zhang, F. Xu, S. Jiang, Wnt signaling in breast cancer: Biological mechanisms, challenges and opportunities. *Mol. Cancer* **19**, 165 (2020).
32. K. R. Brennan, A. M. Brown, Wnt proteins in mammary development and cancer. *J. Mammary Gland Biol. Neoplasia.* **9**, 119–131 (2004).
33. K. J. Gregory *et al.*, Gene expression signature of atypical breast hyperplasia and regulation by SFRP1. *Breast Cancer Res.* **21**, 76 (2019).
34. E. Klopocki *et al.*, Loss of SFRP1 is associated with breast cancer progression and poor prognosis in early stage tumors. *Int. J. Oncol.* **25**, 641–649 (2004).
35. C. Mayer, I. Grummt, Ribosome biogenesis and cell growth: mTOR coordinates transcription by all three classes of nuclear RNA polymerases. *Oncogene* **25**, 6384–6391 (2006).
36. V. Iadevaia, R. Liu, C. G. Proud, mTORC1 signaling controls multiple steps in ribosome biogenesis. *Semin. Cell Dev. Biol.* **36**, 113–120 (2014).
37. E. Dazert, M. N. Hall, mTOR signaling in disease. *Curr. Opin. Cell Biol.* **23**, 744–755 (2011).
38. X. M. Ma, J. Blenis, Molecular mechanisms of mTOR-mediated translational control. *Nat. Rev. Mol. Cell Biol.* **10**, 307–318 (2009).
39. J. D. Richter, N. Sonenberg, Regulation of cap-dependent translation by eIF4E inhibitory proteins. *Nature* **433**, 477–480 (2005).
40. B. Xiao *et al.*, Rheb1-independent activation of mTORC1 in mammary tumors occurs through activating mutations in mTOR. *Cell Rep.* **31**, 107571 (2020).
41. K. Pappas *et al.*, NOTCH and EZH2 collaborate to repress PTEN expression in breast cancer. *Commun. Biol.* **4**, 312 (2021).
42. F. Ades *et al.*, Luminal B breast cancer: Molecular characterization, clinical management, and future perspectives. *J. Clin. Oncol.* **32**, 2794–2803 (2014).
43. W. K. Bae *et al.*, The methyltransferase EZH2 is not required for mammary cancer development, although high EZH2 and low H3K27me3 correlate with poor prognosis of ER-positive breast cancers. *Mol. Carcinog.* **54**, 1172–1180 (2015).
44. M. Wassef, R. Margueron, The multiple facets of PRC2 alterations in cancers. *J. Mol. Biol.* **429**, 1978–1993 (2017).
45. I. Comet, E. M. Riising, B. Leblanc, K. Helin, Maintaining cell identity: PRC2-mediated regulation of transcription and cancer. *Nat. Rev. Cancer* **16**, 803–810 (2016).
46. I. El Ayachi *et al.*, The WNT10B network is associated with survival and metastases in chemoresistant triple-negative breast cancer. *Cancer Res.* **79**, 982–993 (2019).
47. H. Deng *et al.*, CBX6 is negatively regulated by EZH2 and plays a potential tumor suppressor role in breast cancer. *Sci. Rep.* **9**, 197 (2019).
48. E. J. Yeo *et al.*, Myeloid WNT7b mediates the angiogenic switch and metastasis in breast cancer. *Cancer Res.* **74**, 2962–2973 (2014).
49. V. Vafaizadeh *et al.*, The interactions of Bcl9/Bcl9L with beta-catenin and Pygopus promote breast cancer growth, invasion, and metastasis. *Oncogene* **40**, 6195–6209 (2021).
50. D. Buechel *et al.*, Parsing beta-catenin's cell adhesion and Wnt signaling functions in malignant mammary tumor progression. *Proc. Natl. Acad. Sci. U.S.A.* **118**, e2020227118 (2021).
51. M. R. Pool, J. Stumm, T. A. Fulga, I. Sinning, B. Dobberstein, Distinct modes of signal recognition particle interaction with the ribosome. *Science* **297**, 1345–1348 (2002).
52. M. Harachi *et al.*, Dual regulation of histone methylation by mTOR complexes controls glioblastoma tumor cell growth via EZH2 and SAM. *Mol. Cancer Res.* **18**, 1142–1152 (2020).
53. R. Yang *et al.*, E2F7-EZH2 axis regulates PTEN/AKT/mTOR signalling and glioblastoma progression. *Br J. Cancer* **123**, 1445–1455 (2020).
54. J. Chen *et al.*, Long non-coding RNA SNHG1 regulates the Wnt/beta-catenin and PI3K/AKT/mTOR signaling pathways via EZH2 to affect the proliferation, apoptosis, and autophagy of prostate cancer cell. *Front. Oncol.* **10**, 552907 (2020).
55. A. Lanczky, B. Gyorffy, Web-based survival analysis tool tailored for medical research (KMplot): Development and implementation. *J. Med. Internet Res.* **23**, e27633 (2021).
56. L. Liu *et al.*, Ezh2 promotes mammary tumor initiation through the epigenetic regulation of the Wnt and mTORC1 signaling pathways. Gene Expression Omnibus. https://www.ncbi.nlm.nih.gov/geo/query/acc.cgi?acc=GSE2351475. Accessed 16 June 2023.